applied sciences

MDPI

Article

Shear Lag Effect of Ultra-Wide Box Girder under Influence of Shear Deformation

Yanfeng Li [1], Jiyuan Xie [1,*], Fengchi Wang [1] and Yuanhui Li [2]

[1] School of Transportation and Geomatics Engineering, Shenyang Jianzhu University, Shenyang 110168, China; lyfneu@126.com (Y.L.); wfc0914@126.com (F.W.)
[2] School of Resources and Civil Engineering, Northeastern University, Shenyang 110819, China; liyuanhui@126.com
* Correspondence: xiejiyuan0914@126.com

Abstract: The objective of this study was to determine the reasonable flexural functions of ultra-wide box girders, reveal the mechanism of the shear lag effect, and improve the analysis theory of ultra-wide box girders. Considering a single-box three-chamber thin-walled box girder as an example, starting from an uneven transfer of shear flow, the flexural displacement function of the curved box girder under the influence of shear deformation of each plate was derived according to the flexural theory of a thin-walled box girder, balance equation of a thin-walled microelement plate, and theory of plane stress. The energy variational method was used to analyze the flexural displacement function, providing a theoretical solution for the shear lag effect of the curved box girder. A displacement correction of the cantilever plate displacement function was performed by comparing the calculation results for the shear lag coefficients. The results indicated that under the shear deformation of each plate, the flexural displacement functions of the wing and web plates of the box girder no longer satisfy the assumption of plane section. The flexural displacement function is a quadratic function of the transverse wing plate, and the web height is the sum of the first- and third-order functions. The theoretical calculation results agree sufficiently well with the experimental results, proving that the flexural displacement function of the box girder under the influence of the shear deformation of each plate is reliable.

Keywords: wide thin-walled box girder; uneven transfer of shear flow; flexural displacement function; shear lag effect

check for updates

Citation: Li, Y.; Xie, J.; Wang, F.; Li, Y. Shear Lag Effect of Ultra-Wide Box Girder under Influence of Shear Deformation. *Appl. Sci.* **2024**, *14*, 4778. https://doi.org/10.3390/app14114778

Academic Editor: Sang-Hyo Kim

Received: 23 March 2024
Revised: 13 May 2024
Accepted: 28 May 2024
Published: 31 May 2024

Copyright: © 2024 by the authors. Licensee MDPI, Basel, Switzerland. This article is an open access article distributed under the terms and conditions of the Creative Commons Attribution (CC BY) license (https://creativecommons.org/licenses/by/4.0/).

1. Introduction

Considering the development of bridge structures using light thin-wall, long-span, wide-web spacings and wide cantilever plates, problems related to the spatial mechanics caused by thin-walled structures have become increasingly prominent [1–3]. When the thin-walled box girder is in a flexural state, the flexural function of the wing plate is no longer applicable to the assumption of the plane section owing to the influence of shear deformation; the resulting warping phenomenon is called the "shear lag effect" [4–6].

The analytical method based on the principle of energy variation is a research approach rooted in the theory of elasticity. Among various methods employed for analyzing the shear lag effect in box girders, the energy variation method stands out as the most commonly utilized. This method involves treating the difference between the longitudinal displacements of the girder body and the longitudinal displacements of the wing plates as unknowns. By applying the minimum potential energy theory to resolve the governing differential equations, the deflection of the girder body and the transverse distribution of normal stresses can be obtained. Wei et al. [7] expressed the shear lag deflection function using the maximum shear deformation difference function, and combined it with the energy variation method to investigate the shear lag effect in curved box girders. Wang et al. [8] assumed the shear lag deflection functions of box beams on the cantilever, top, and bottom

plates. Based on spline finite points and the principle of energy variation, they discretized the structure using B-spline curve equations, thus revealing the variation law of shear lag effect in box girders. Chen et al. [9], on the foundation of energy variation theory, introduced spatial girder element functions and derived the Euler girder matrix equation. By considering the influence of shear deformation, they derived the stiffness matrix of Timoshenko beams. Through extensive exploration by numerous scholars, the domain of energy variation methods has been further expanded. From rectangular box sections to curved box girder sections, and then to box girders utilizing composite materials, it has been discovered that employing the energy variation method to solve for the shear lag effect is indeed feasible. This paper also aims to investigate the shear lag effect in thin-walled box girders using the energy variation method. The key issue lies in accurately determining the form of the deflection function, as it directly affects the precision of solving for the shear lag effect.

Currently, the flexural displacement function is primarily based on artificial assumptions and has been considered quadratic parabola, cubic parabola, quadric parabola, cosine function, and catenary-type [10–14] functions. Lin et al. [15] reported that the shear lag effect of thin-walled box girders was essentially caused by shear deformation. By studying the shear flow of a box girder under a vertical load, they proposed a flexural displacement function with shear deformation. Penalba et al. [16]. represented the shear strain of a steel–concrete composite girder with a cosine function and established a mechanical analysis model of a steel–concrete composite girder considering the influence of shear deformation and interface slip between the concrete and steel plate [17]. The proposed model was verified by comparing the obtained results with solutions of elastic analysis and finite-element results. Zhang et al. [18] introduced boundary correction factors to the cantilever plate to reflect the influence of different boundary constraints on the shear lag deflection. By utilizing spatial finite-element software to compute the results, the values of the boundary correction factors for the cantilever plate were determined. Many domestic and international scholars have also established sophisticated bridge finite-element models, verifying their simulation results through dual validation against experiments [19–22].

In the literature, the theoretical methods for flexural analysis of thin-walled box girders mainly focus on the shear lag effect of the box girders, whereas research on flexural and shear deformation is lacking [23]. In particular, the theoretical correlation between the elementary beam theory and spatial mechanics analysis theory of box girders under the influence of shear deformation of each plate is limited. In this study, the flexural displacement function of a box girder under the influence of shear deformation of each plate is proposed, and the spatial mechanics analysis theory of box girders is improved. This paper will also conduct a comparative analysis of the deflection stress calculation results and propose a cantilever displacement correction for the bending deflection function of thin-walled box girders considering the effects of shear deformation in each plate. A solid model of a single-box three-chamber box girder will be established using MIDAS/FEA NX 2021 finite-element software to analyze the factors influencing the shear lag effect under different loading conditions. The theoretical solution for the shear lag effect in the bent box girder will be provided based on the energy variation method to analytically derive the deflection function. Factors affecting the shear lag effect will be introduced to modify the formula for the shear lag effect in a single-box three-chamber box girder, addressing the workload issue in internal force calculations for box girders.

The innovative aspects of this article include theoretically deriving the deflection function of thin-walled box girders under bending, influenced by the shear deformation of each plate, due to uneven shear flow transfer. This also leads to a theoretical analysis of wide-span box girders under the effect of uneven shear flow transfer. The theoretical solutions and influencing factors of the shear lag effect in bent box girders are solved using the energy variation method. Using Origin, an empirical formula for the shear lag effect in a single-box three-chamber girder is fitted, addressing the problem of calculating internal forces in box girders.

2. Analysis of Flexural Displacement Function of Flexural Box Girder under Shear Deformation of Plates

Considering the main girder with a single box and three chambers as the object of analysis, the force diagram of a thin-walled box girder under an arbitrary vertical load distribution is shown in Figure 1. The section coordinates and dimensions of the box girder are shown in Figure 2, where the center of the cross-section is the origin of the coordinate system, and the main inertial axes of the section are the coordinate axes.

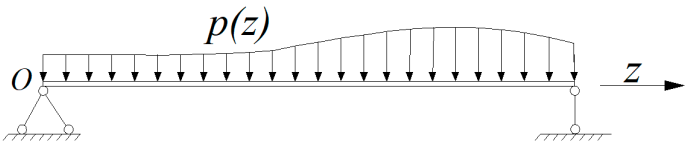


Figure 1. Loading force diagram.

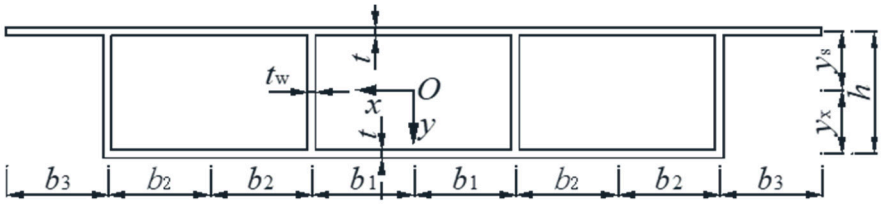


Figure 2. Coordinates and size diagram of a single-box three-chamber box girder section.

In thin-walled box girders, stress is assumed to be uniformly distributed along the wall thickness direction. For the study of thin-walled box girders, the position of any point on the section can be represented by the coordinates of the flow curve along the centerline of the thickness of the box wall, and the section of the thin-walled box girder can be simplified. A simplified section of the thin-walled box girder is shown in Figure 3, wherein the right-hand flow coordinate system is formed using n, s, and z; u represents the displacement of the longitudinal z-axis of the girder body, and v represents the displacement of the circumferential s-axis of the girder wall.

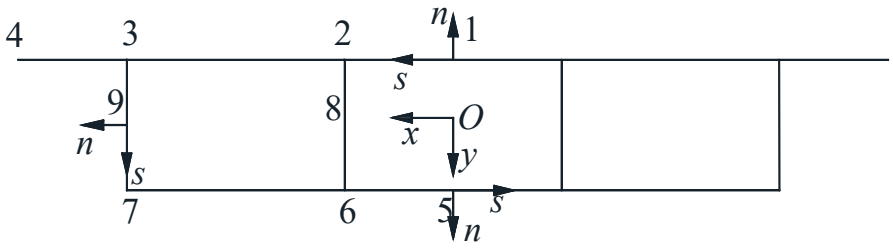


Figure 3. Simplified schematic of the box girder sections.

The following basic assumptions were made according to the flexural theory of a box girder [24,25]:

(1) Under small-deformation conditions, the contour projection of the box girder section does not deform.

(2) The strain ε_s at the midpoint of each plate is zero; that is, for each plate of the box girder, $\partial v/\partial s = 0$.

(3) The shear deformation outside the plane of each plate of the box girder is not considered, that is, $\tau_{nz} = 0, \sigma_n = 0$.

In Figure 3, 1 is the center point of the top plate of the inner chamber, 2 is the apex of the inner web, 3 is the apex of the outer web, 4 is the outer edge point of the cantilever plate, 5 is the center point of the bottom plate of the inner chamber, 6 is the bottom point of the inner web, 7 is the bottom point of the outer web, 8 is the intersection point of the centroidal x-axis and inner web, and 9 is the intersection of the centroidal x-axis and outer web.

To study the equilibrium state of the thin-walled member, microplates with a certain thickness were obtained from the cross-section of the thin-walled box girder, and the thin-walled microplates are shown in Figure 4. As the structure is in a flexural state, normal and shear stresses exist in the microplates; according to the principle of shear stress reciprocity, $\tau_{sz} = \tau_{zs} = \tau$. In addition, because the thickness of the microplate in section dz is constant, the shear force $q = \tau t$ of the unit length along the cross-section of the wall plate can be determined. This is called the shear flow; its flow direction is the same as that of s.

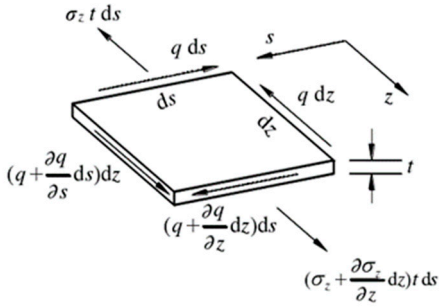


Figure 4. Diagram of the thin-walled element.

According to the mechanical equilibrium conditions, the resultant force of the thin-walled element shown in Figure 4 is zero along the z-axis:

$$\left(\sigma_z + \frac{\partial \sigma_z}{\partial z}\mathrm{d}z\right)t\mathrm{d}s - \sigma_z t\mathrm{d}s + \left(q + \frac{\partial q}{\partial s}\mathrm{d}s\right)\mathrm{d}z - q\mathrm{d}z = 0. \tag{1}$$

By simplifying Equation (1), we obtain

$$\frac{\partial \sigma_z}{\partial z}t + \frac{\partial q}{\partial s} = 0. \tag{2}$$

The basic assumption does not consider the out-of-plane shear deformation of each plate of the box girder, and $\tau_{nz} = 0, \sigma_n = 0$ indicates that each plate is in a state of plane stress. According to the theory of elasticity, the following can be obtained:

$$\frac{\partial u}{\partial z} = \varepsilon_z \tag{3}$$

$$\frac{\partial v}{\partial s} = \varepsilon_s \tag{4}$$

$$\gamma_{sz} = \frac{\partial u}{\partial z} + \frac{\partial v}{\partial s}. \tag{5}$$

The stress distribution in the thin-walled box girder under shear deformation is not clear; therefore, it cannot be calculated using the microelement equilibrium Equations (1)–(5). To solve this problem, we assume that the displacement function is the same as that of the elementary girder to obtain the flexural shear stress of the box girder using the microelement equilibrium equation; the assumed flexural displacement is then modified.

Under the assumption of a plane section, the equation for the flexural normal stress σ_z of the box girder is as follows [26]:

$$\sigma_z = \frac{M(z)}{I_x}y, \tag{6}$$

where $M(z)$ represents the bending moment of the box girder (N·m), y represents the distance from the transverse spindle of the box girder (m), and I_x represents the inertia distance of the box girder section with respect to the x-axis (m^4).

According to the flexural theory of thin-walled structures with openings [27], Equation (6) is substituted into Equation (2) to simplify the expression of the shear flow [28]:

$$q(s) = -\frac{M'(z)}{I_x} S_y, \tag{7}$$

where $q(s)$ represents the flexural shear flow and S_y represents the distance of the cross-section of the net area with respect to the y-axis.

Because the section of the box girder is a statically indeterminate structure $\bar{q}$, to determine the initial shear flow at any starting point, a cut can be set at any section of the box girder to convert it into a statically indeterminate open-section problem for obtaining the initial value of the shear flow $\bar{q}$. By superimposing the open-section shear flow q_0 and additional shear flow q_i, the closed-section shear flow q can be obtained as follows:

$$q(s) = q_0 + q_i. \tag{8}$$

The cross-sectional size of the single-box three-chamber box girder is shown in Figure 5a; the shear center of the section is influenced by the bending moment $M(z)$. Virtual incisions were made on the sections of each closed-box chamber. The locations of the virtual incisions are shown in Figure 5b. The calculation equation for the shear flow in the open section is as follows:

$$q_0 = -\frac{M'(z)}{I_x} S_y = -\frac{M'(z)}{I_x} \int yt\mathrm{d}s. \tag{9}$$

Figure 5c presents the distribution of the shear flow q_0 in the open sections of the three chambers in a single box girder. The arrow indicates the direction of the actual shear flow, which is obtained by combining the shear flow direction and the integral direction of the static surface moment.

According to a previous study [29], if the incision selected is at the top and bottom plates on the sectional symmetry axis, the calculation of the shear flow in statically indeterminate structures can be obtained from the deformation compatibility conditions.

The deformation compatibility condition of chamber i is expressed as

$$\oint_i \frac{q_0}{t}\mathrm{d}s + q_i \oint_i \frac{\mathrm{d}s}{t} - \sum q_k \int_{i.k} \frac{\mathrm{d}s}{t} = 0, \tag{10}$$

where q_0 represents the basic shear flow in the open section, q_i represents the additional shear flow in chamber i, and q_k represents the additional shear flow in the adjacent chamber.

The additional shear flow q_i in each chamber is solved according to the deformation compatibility condition, as shown in Figure 5d. By superimposing Figure 5c,d, the shear flow in the section of a single box and three chambers is obtained, and the corresponding shear flow distribution is shown in Figure 5e.

Considering the top plate #1 of the box girder as an example, its internal shear deformation was analyzed, and its shear flow equation was obtained as follows:

$$q(s) = \frac{M'(z)}{I_x} y_s t s + q_2, \tag{11}$$

where y_s represents the distance between the centerline of the top plate and the x-axis of the center of the box girder section, and q_2 represents the additional shear flow in chamber 2.

When the box girder is bent, the displacement of the top plate along the perimeter s is zero, and $v(z) = 0$ according to the basic assumption; thus, $\partial v/\partial z = 0$. According to Equations (5) and (11),

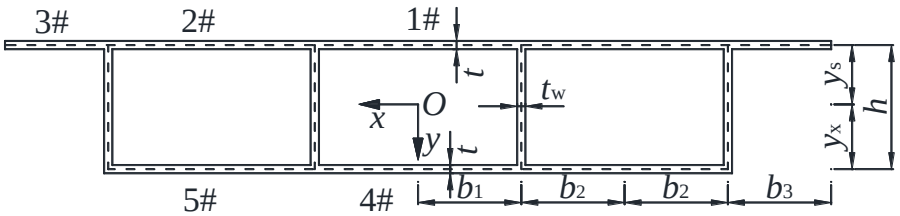
$$\gamma_{sz} = \frac{\partial u}{\partial s} = \frac{\tau_{sz}}{G} = \frac{q(s)}{Gt} = \frac{M'(z) y_s}{G I_x} s + \frac{q_2}{Gt}, \tag{12}$$

where G represents the shear modulus of elasticity.

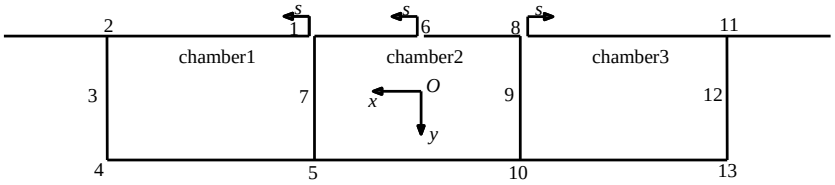
The equation for the longitudinal displacement of the top plate of the box girder #1 can be obtained by introducing s into Equation (12) as follows:

$$u(s,z) = u_0(s,z) + u_i(s,z) = \frac{M'(z)y_s}{2GI_x}s^2 + \frac{q_2}{Gt}s + u_{01}(z), \tag{13}$$

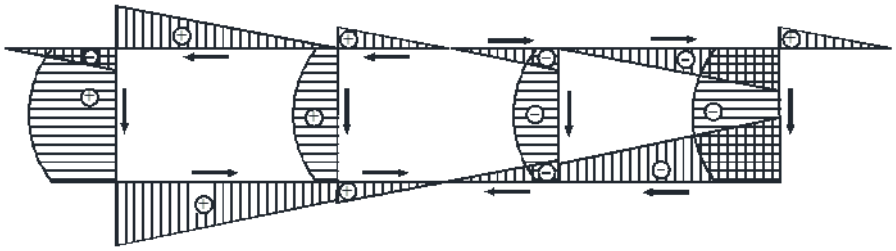
where $u_{01}(z)$ represents the longitudinal displacement of the center of the top plate of the box girder (starting point of coordinate s).



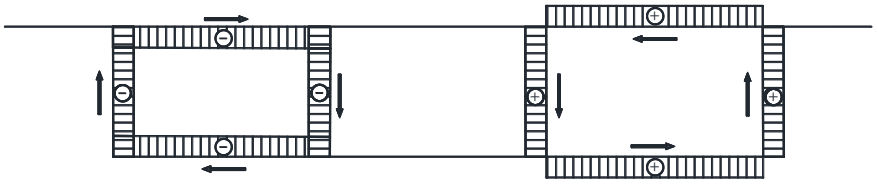
(**a**) Sectional dimensions and plate division.



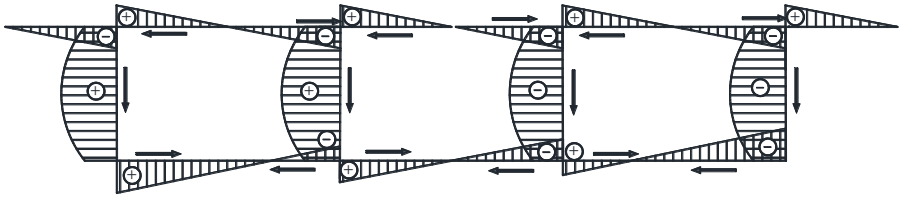
(**b**) Virtual incision diagram.



(**c**) Distribution diagram of the shear flow q_0 in an open section.



(**d**) Diagram of the girder with an additional shear flow.



(**e**) Shear flow diagram.

Figure 5. Shear flow diagram of a single-box three-chamber girder.

The expression of the longitudinal displacement at the inner web apex 2 (see Figure 3) can be obtained via the simplified Equation (13) as follows:

$$u_{02}(z) = \frac{M'(z)y_s}{2GI_x}{b_1}^2 + u_{01}(z) \tag{14}$$

if

$$g_{01}(z) = u_{02}(z) - u_{01}(z) = \frac{M'(z)y_s}{2GI_x}{b_1}^2, \tag{15}$$

where b_1 represents the width of plate #1.

By substituting Equations (14) and (15) into Equation (13) and replacing s representing the horizontal position in the equation with the x coordinate, we obtain

$$u(x,z) = u_{02}(z) - \left(1 - \frac{x^2}{{b_1}^2}\right)g_1(z) - \beta_1(z)\left(1 - \frac{x}{b_1}\right) \tag{16}$$

Considering center point 5 of the bottom plate of the box girder (see Figure 3) as the integral starting point of plate #4 (bottom plate of inner chamber), the equation for longitudinal displacement of plate #4 can be obtained as follows:

$$u(x,z) = u_{06}(z) - \left(1 - \frac{x^2}{{b_1}^2}\right)g_1(z) - \beta_1(z)\left(1 - \frac{x}{b_1}\right), \tag{17}$$

where $\beta_1(z) = \frac{q_2}{Gt}b_1$.

Similarly, the longitudinal displacement equations of the other wall plates can be obtained. The longitudinal displacement equations for the top and bottom plates are as follows:

$$u(x,y,z) = \begin{cases} u_2(z) - y_s\left({b_1}^2 - x^2\right)g(z) - \frac{2q_2}{t}(b_1 - x)g(z) & \text{Plate\#1} \\ u_6(z) + y_x\left({b_1}^2 - x^2\right)g(z) - \frac{2q_2}{t}(b_1 - x)g(z) & \text{Plate\#4} \\ u_3(z) - y_s\left[4{b_2}^2 - (b_1 + 2b_2 - x)^2\right]g(z) - \frac{2q_1}{t}[2b_2 - (b_1 + 2b_2 - x)]g(z) & \text{Plate\#2} \\ u_7(z) + y_x\left[4{b_2}^2 - (b_1 + 2b_2 - x)^2\right]g(z) - \frac{2q_1}{t}[2b_2 - (b_1 + 2b_2 - x)]g(z) & \text{Plate\#5} \\ u_3(z) - y_s\left[{b_3}^2 - (b_1 + 2b_2 + b_3 - x)^2\right]g(z) & \text{Plate\#3} \end{cases} \tag{18}$$

According to Equation (18), the flexural displacements of the top plate of the inner chamber (plate#1), top plate of the outer chamber (plate#2) and cantilever plate (plate#3), bottom plate of the inner chamber (plate#4), bottom plate of the outer chamber (plate#5) can be represented by $u_2(z)$, $u_3(z)$, $u_6(z)$, and $u_7(z)$, respectively.

As shown in Figure 5, the distribution of the shear flow on the box girder web is a quadratic function. By analyzing the shear flow on the box girder web, the shear flows $q_8(z)$ and $q_9(z)$ at points 8 and 9 (see Figure 3) of the box girder web can be obtained as follows:

$$q_8(z) = q_{08}(z) + (q_1 - q_2) = \frac{M'(z)}{I_x}y_s A_{s1} + \frac{M'(z)}{2I_x}{y_s}^2 t_w + (q_1 - q_2) \tag{19}$$

$$q_9(z) = q_{09}(z) + q_1 = \frac{M'(z)}{I_x}y_s A_{s2} + \frac{M'(z)}{2I_x}{y_s}^2 t_w + q_1, \tag{20}$$

where t_w represents the web thickness and A_{si} represents the area of the wing plate corresponding to the open-section web.

According to Equations (19) and (20), the flexural shear flow at any point of the box girder web can be expressed as follows:

$$q(y,z) = q_{8,9}(z) - \frac{M'(z)}{2I_x}y^2 t_w. \tag{21}$$

The web shear deformation equation obtained from Equations (5) and (21) is as follows:

$$\gamma_{sz} = \frac{\partial u}{\partial s} + \frac{\partial v}{\partial z} = \frac{q(z)}{Gt_w} = \frac{q_{8,9}(z)}{Gt_w} - \frac{M'(z)}{2GI_x}y^2. \tag{22}$$

According to the rigid peripheral assumption, if $w(z)$ is the vertical flexural displacement of the girder body, the relationship between the flexural angle of the box girder and the circumferential displacement of the web plate is as follows:

$$w'(z) = \frac{\partial v}{\partial z}. \tag{23}$$

Equation (22) is substituted into Equation (23) and s is replaced with y to represent the position of any vertical point on the web. After simplification of the integral, the equation for the flexural longitudinal displacement at any point on the box girder web is obtained as follows:

$$u(y,z) = -yw'(z) + (\frac{q_{08,09}(z)}{Gt_w} + \frac{q_i}{Gt_w})y - \frac{M'(z)}{6GI_x}y^3 + u_{8,9}(z). \tag{24}$$

By simplifying Equations (19), (20) and (24), $u_2(z)$, $u_3(z)$, $u_6(z)$, and $u_7(z)$ are obtained. By combining Equations (18)–(20) and (24), the flexural longitudinal displacements of the box girder represented by $u_8(z)$ and $u_9(z)$ are obtained, the equations for which are presented below.

Inner chamber top and bottom plates and inner web:

$$u(x,y,z) = -yw'(z) + \left[\alpha_1 y - \frac{1}{3}y^3 + \eta_1(x,y)\right]g(z) + u_8(z) \tag{25}$$

Outer chamber top and bottom plates, cantilever plate, and outer web plate:

$$u(x,y,z) = -yw'(z) + \left[\alpha_2 y - \frac{1}{3}y^3 + \eta_2(x,y)\right]g(z) + u_9(z) \tag{26}$$

where $\alpha_1 = \frac{2y_s A_{s1}}{t_w} + {y_s}^2 + \frac{2(q_1-q_2)}{t_w}$; $\alpha_2 = \frac{2y_s A_{s2}}{t_w} + {y_s}^2 + \frac{2q_1}{t_w}$.

$\eta_1(x,y)$ and $\eta_2(x,y)$; the equation is as follows:

$$\eta_1(x,y) = \begin{cases} -y_s\left({b_1}^2 - x^2\right) - \frac{2q_2}{t}(b_1 - x) & \text{Plate\#1} \\ y_x\left({b_1}^2 - x^2\right) - \frac{2q_2}{t}(b_1 - x) & \text{Plate\#4} \end{cases} \tag{27}$$

$$\eta_2(x,y) = \begin{cases} -y_s\left[4{b_2}^2 - (b_1 + 2b_2 - x)^2\right] - \frac{2q_1}{t}[2b_2 - (b_1 + 2b_2 - x)] & \text{Plate\#2} \\ -y_s\left[{b_3}^2 - (b_1 + 2b_2 + b_3 - x)^2\right] & \text{Plate\#3} \\ y_x\left[4{b_2}^2 - (b_1 + 2b_2 - x)^2\right] - \frac{2q_1}{t}[2b_2 - (b_1 + 2b_2 - x)] & \text{Plate\#5} \end{cases}. \tag{28}$$

Equations (27) and (28) indicate that the flexural longitudinal displacement function of the box girder includes the longitudinal displacements $u_8(z)$ and $u_9(z)$ of the inner and outer webs at the x-axis of the centroid and the intersection point. To accurately analyze the flexural longitudinal displacement function of the box girder under the influence of shear deformation of each plate, the longitudinal displacements $u_8(z)$ and $u_9(z)$ should be analyzed correctly.

Because the sum of the stresses on the box girder cross-section in the flexural state is zero, the following can be obtained:

$$F_N = \int_A \sigma_z dA = 0. \tag{29}$$

According to Hooke's law and Equation (3), the normal stress $\sigma(x,y,z)$ at any point on the section of the flexural box girder can be expressed as follows:

$$\sigma(x,y,z) = E\varepsilon_z = E\frac{\partial u}{\partial z}. \tag{30}$$

By substituting Equations (25) and (26) into Equation (30), Equation (31) can be obtained as follows:

$$\begin{array}{l} F_N = E\int_{A_1}\left\{-yw''(z)+\left[\alpha_1 y-\frac{1}{3}y^3+\eta_1(x,y)\right]g'(z)+u'_8(z)\right\}dA+ \\ E\int_{A_1}\left\{-yw''(z)+\left[\alpha_2 y-\frac{1}{3}y^3+\eta_2(x,y)\right]g'(z)+u'_9(z)\right\}dA=0 \end{array}. \tag{31}$$

Equation (31) is simplified, and F_N decomposes into the following:

$$F_{N1} = -w''(z)E\int_A ydA \tag{32}$$

$$F_{N2} = \alpha_i g'(z)E\int_A ydA \tag{33}$$

$$F_{N3} = -\frac{1}{3}g'(z)E\int_A y^3dA \tag{34}$$

$$F_{N4} = Eg'(z)\int_{A1}\eta_1(x,y)dA \tag{35}$$

$$F_{N5} = Eg'(z)\int_{A2}\eta_2(x,y)dA \tag{36}$$

$$F_{N6} = u'_8(z)E\int_{A1}dA \tag{37}$$

$$F_{N7} = u'_9(z)E\int_{A2}dA. \tag{38}$$

The static moment of the x-axis at the center of the box girder section as well as the integral results of Equations (32) and (33) are zero. If the sum of the stresses is zero, that is, if Equation (31) holds, the sum of Equations (34)–(38) is zero. According to this relationship, the following can be obtained:

$$A_1u'_8(z)+A_2u'_9(z) = -\left[\int_{A1}\eta_1(x,y)dA+\int_{A2}\eta_2(x,y)dA+\frac{1}{3}\int_A y^3dA\right]g'(z). \tag{39}$$

By integrating both sides with respect to z, the following is obtained:

$$A_1u_8(z)+A_2u_9(z) = dg(z)+C, \tag{40}$$

where C is the integration constant. Because the girder body does not expand in the axial direction under a bending load, $C = 0$; d is the shear lag warpage function that satisfies the axial balance parameter of Equation (31).

$$d = d_e + d_w. \tag{41}$$

$$d_e = \frac{2\left[(y_sA_t-y_xA_b)\left({b_1}^2+4{b_2}^2\right)+(A_t-A_b)\left(\frac{2q_2}{t}b_1+\frac{2q_1}{t}2b_2\right)+y_sA_c{b_3}^2\right]}{3A} \tag{42}$$

$$d_w = \frac{\left[{y_x}^3A_b-{y_s}^3(A_t+A_c)+\frac{t_w}{2}\left({y_x}^4-{y_s}^4\right)\right]}{3A} \tag{43}$$

Here, A_t represents the cross-sectional area of the top plate, A_b represents the cross-sectional area of the bottom plate, and A_c represents the cross-sectional area of the cantilever.

According to Equations (25), (26) and (40), under the influence of the shear deformation of the plate, the neutral axis of the box girder section no longer overlaps with the centroidal axis, and the deviation distance from the centroidal axis is $d \times g(z)$.

According to the aforementioned description, after $u_8(z)$ and $u_9(z)$ are substituted into Equations (25) and (26) and the axial balance parameter d is substituted into $\eta_1(x,y)$ and

$\eta_2(x,y)$, the flexural displacement function of the flexural box girder under the influence of the shear deformation of each plate is expressed as follows:

$$u(x,y,z) = -yw'(z) + \left[\alpha_i y - \frac{1}{3}y^3 + \eta_\zeta(x,y)\right]g(z). \tag{44}$$

In Equation (44), $\eta_\zeta(x,y)$ is given as follows:

$$\eta_\zeta(x,y) = \begin{cases} -y_s\left({b_1}^2 - x^2\right) - \frac{2q_2}{t}(b_1 - x) + k_1 d & \text{Plate\#1} \\ y_x\left({b_1}^2 - x^2\right) - \frac{2q_2}{t}(b_1 - x) + k_1 d & \text{Plate\#4} \\ -y_s\left[4{b_2}^2 - (b_1 + 2b_2 - x)^2\right] - \frac{2q_1}{t}[2b_2 - (x - b_1)] + k_2 d & \text{Plate\#2} \\ y_x\left[4{b_2}^2 - (b_1 + 2b_2 - x)^2\right] - \frac{2q_1}{t}[2b_2 - (x - b_1)] + k_2 d & \text{Plate\#5} \\ -y_s\left[{b_3}^2 - (b_1 + 2b_2 + b_3 - x)^2\right] + k_2 d & \text{Plate\#3} \\ \\ k_1 d & \text{Inner web} \\ k_2 d & \text{Outer web} \end{cases}. \tag{45}$$

where k_1 and k_2 are the axial balance coefficients of the web, which are determined by the shear distribution law of the web and the ratio of A_1 to A_2.

3. Analysis of Flexural Displacement Function of Box Girder via Energy Variational Method

According to the flexural displacement function of the flexural thin-walled box girder under the shear deformation of each plate, the energy variational principle [30,31] was applied to analyze the flexural displacement function of the thin-walled box girder. Using Equation (44), the longitudinal strain equation for each point of the thin-walled box girder section can be obtained as follows:

$$\varepsilon_z = \frac{\partial u}{\partial z} = -y\omega''(z) + \left[\alpha y - \frac{1}{3}y^3 + \eta_\zeta(x,y)\right]g'(z) = -y\omega''(z) + \eta(x,y)g'(z). \tag{46}$$

The shear strain of each wing plate is expressed as follows:

$$\gamma_{xz} = \frac{\partial u}{\partial x} = \frac{\partial \eta_\zeta(x,y)}{\partial x}g(z). \tag{47}$$

The shear strain of each web is expressed as follows:

$$\gamma_{yz} = \frac{\partial u}{\partial s} + \frac{\partial v}{\partial z} = \frac{\partial u}{\partial y} + \omega'(z) = \frac{\partial \eta(x,y)}{\partial y}g(z). \tag{48}$$

According to the energy variational principle, the positive strain energy of each plate of the box girder under flexural deformation can be expressed as follows:

$$U_1 = \frac{1}{2}\iint \sigma_z \varepsilon_z dAdz = \frac{E}{2}\iint {\varepsilon_z}^2 dAdz. \tag{49}$$

The flexural shear strain energy of each plate of the box girder is given as

$$U_2 = \frac{1}{2}\iint (\tau_{xz}\gamma_{xz} + \tau_{yz}\gamma_{yz})dAdz = \frac{G}{2}\iint \left({\gamma_{xz}}^2 + {\gamma_{yz}}^2\right)dAdz \tag{50}$$

By substituting Equations (46)–(48) into Equations (49) and (50), the total strain energy of the box girder under flexural deformation can be obtained as follows:

$$U = \frac{1}{2}\int_l \int_A \left(E\varepsilon^2 + G\gamma^2\right) dAdz = \frac{1}{2}\int_l \left[EI_x{\omega''}^2 + EI_\eta g' - 2EI_{y\eta}\omega'' g' + G\left(A_x + A_y\right)g^2\right] dz \tag{51}$$

where I_η represents the cross-sectional warping moment of inertia, A_x represents the shear warping moment of the wing plate, and A_y represents the shear buckling moment of the web. The parameter equation of the shear warping sections defined in this study is as follows:

$$\begin{aligned} A_x = \int_A \left(\frac{\partial \eta_\zeta}{\partial x}\right)^2 dA = \frac{1}{3}\Big\{ & A_t\left[(y_s 2b_1 + 2q_2/t)^2 + (4b_2 y_s + 2q_1/t)^2\right] + \\ & A_b\left[(y_x 2b_1 + 2q_2/t)^2 + (4b_2 y_x + 2q_1/t)^2\right] + A_c(y_s 2b_3)^2\Big\} \end{aligned} \tag{52}$$

$$A_y = \int_A \left(\frac{\partial \eta}{\partial y}\right)^2 dA = \alpha^2 A_w + I_{4w} - \alpha I_{2w} \tag{53}$$

$$I_\eta = \int_A \eta(x,y)^2 dA = \alpha^2 I_x + \frac{1}{9}I_6 + I_\zeta - \frac{2}{3}\left(\alpha I_4 - 3\alpha I_{1\zeta} + I_{3\zeta}\right) \tag{54}$$

$$I_{y\eta} = \int_A y\eta(x,y) dA = \alpha I_x - \frac{1}{3}I_4 + I_{1\zeta} \tag{55}$$

$$I_n = \int_A y^n dA = {y_s}^n(A_t + A_c) + {y_x}^n A_b + \frac{4t_w\left({y_s}^{n+1} + {y_x}^{n+1}\right)}{n+1}, (n = 4, 6) \tag{56}$$

$$I_{nw} = \int_A y^n dA_w = \frac{4t_w\left({y_s}^{n+1} + {y_x}^{n+1}\right)}{n+1}, (n = 2, 4) \tag{57}$$

$$\begin{aligned} I_\zeta = {} & \int_A \eta_\zeta(x,y)^2 dA = \left(A_1{k_1}^2 + A_2{k_2}^2\right)d^2 + \\ & A_t\left\{\begin{array}{l} \frac{8}{15}\left[{y_s}^2{b_1}^4 + \left(\frac{q_2 b_1}{t}\right)^2 + {y_s}^2\left(4{b_2}^2\right)^2 + \left(\frac{2q_1 b_2}{t}\right)^2 + \left(\frac{2q_3 b_2}{t}\right)^2\right] - \\ \frac{4}{3}\left(y_s k_1 d{b_1}^2 + y_s k_2 d4{b_2}^2 - \frac{4y_s q_2 {b_1}^3}{t} - \frac{8y_s q_1 {b_2}^3}{t} - \frac{8y_s q_3 {b_2}^3}{t} + \frac{4k_1 d q_2 b_1}{t} + \frac{4k_2 d q_1 b_2}{t} + \frac{4k_2 d q_3 b_2}{t}\right) \end{array}\right\} + \\ & A_b\left\{\begin{array}{l} \frac{8}{15}\left[{y_x}^2{b_1}^4 + \left(\frac{q_2 b_1}{t}\right)^2 + {y_x}^2\left(4{b_2}^2\right)^2 + \left(\frac{2q_1 b_2}{t}\right)^2 + \left(\frac{2q_3 b_2}{t}\right)^2\right] + \\ \frac{4}{3}\left(y_x k_1 d{b_1}^2 + y_x k_2 d4{b_2}^2 - \frac{4y_x q_2 {b_1}^3}{t} - \frac{8y_x q_1 {b_2}^3}{t} - \frac{8y_x q_3 {b_2}^3}{t} + \frac{4k_1 d q_2 b_1}{t} + \frac{4k_2 d q_1 b_2}{t} + \frac{4k_2 d q_3 b_2}{t}\right) \end{array}\right\} + \\ & A_c y_s\left(\frac{8}{15}y_s{b_3}^2 - \frac{4}{3}k_2 d\right){b_3}^2 \end{aligned} \tag{58}$$

$$I_{n\zeta} = \int_A y^n \eta_\zeta(x,y) dA = \frac{2}{3}{y_s}^{n+1}\left[A_t\left({b_1}^2 + 4{b_2}^2\right) + A_c{b_3}^2 + A_b\left({b_1}^2 + 4{b_2}^2\right)\left(\frac{y_x}{y_s}\right)^{n+1}\right], (n = 1, 3). \tag{59}$$

where A_t represents the area of the top plate, A_b represents the area of the bottom plate, A_c represents the area of the cantilever plate, A_w represents the area of the unilateral web, and A represents the full-section area of the box girder.

The potential energy V owing to the external load of the thin-walled box girder is expressed as follows:

$$V = -\int_l M(z)\omega''(z) dz. \tag{60}$$

From Equations (51) and (60), the total bending potential energy of the box girder can be obtained as follows:

$$\prod = U + V = \frac{1}{2}\int_l \left[EI_x\omega''^2 + EI_\eta g'^2 - 2EI_{y\eta}\omega'' g' + G\left(A_x + A_y\right)g^2\right]dz - \int_l M(z)\omega''(z)dz. \tag{61}$$

According to the principle of the minimum potential energy, the stationary value $\delta\prod = 0$ is substituted into Equation (61), yielding

$$\begin{aligned}\delta\prod &= \int_l \left[EI_x\omega''\delta\omega'' + EI_\eta g'\delta g' - EI_{y\eta}(\omega''\delta g' + g'\delta\omega'') + G\left(A_x + A_y\right)g\delta g + M\delta\omega''\right]dz \\ &= \int_l \left[\left(EI_x\omega'' - EI_{y\eta}g' + M\right)\delta\omega'' + \left(EI_\eta g' - EI_{y\eta}\omega''\right)\delta g' + G\left(A_x g + A_y g\right)\delta g\right]dz\end{aligned} \tag{62}$$

Integration by parts, i.e., $\int_a^b udv = [uv]_a^b - \int_a^b vdu$, is used to solve (62), and the following is obtained:

$$\begin{aligned}\delta\prod &= \int_l \left[\left(EI_x\omega'' - EI_{y\eta}g' + M\right)\delta\omega'' + \left(EI_\eta g' - EI_{y\eta}\omega''\right)\delta g' + G\left(A_x g + A_y g\right)\delta g\right]dz \\ &= \int_l \left\{\left(EI_x\omega'' - EI_{y\eta}g' + M\right)\delta\omega'' + \left[G\left(A_x g + A_y g\right) - EI_\eta g'' + EI_{y\eta}\omega'''\right]\delta g\right\}dz + \left(EI_\eta g' - EI_{y\eta}\omega''\right)\delta g\ |_0^l\end{aligned}. \tag{63}$$

According to the principle of the variational method and Equation (63), the control differential equation for the flexural box girder can be obtained as follows:

$$EI_x\omega'' - EI_{y\eta}g' + M = 0 \tag{64}$$

$$G\left(A_x g + A_y g\right) - EI_\eta g'' + EI_{y\eta}\omega''' = 0. \tag{65}$$

The resulting boundary conditions are as follows:

$$\left(EI_\eta g' - EI_{y\eta}\omega''\right)\delta g\ |_0^l = 0. \tag{66}$$

By simplifying Equations (64) and (65), we obtain the following:

$$g'' - k^2 g = -k_0 Q(z) \tag{67}$$

$$\omega'' = -\frac{M}{EI_x} + Bg'. \tag{68}$$

Here, $B = I_{y\eta}/I_x$, and $k = \sqrt{\frac{G\left(A_x + A_y\right)I_x}{E\left(I_x I_\eta - I_{y\eta}{}^2\right)}}$ and $k_0 = \frac{I_{y\eta}}{E\left(I_x I_\eta - I_{y\eta}{}^2\right)}$ are shear parameters.

By solving Equation (63), the general solution for the shear displacement is obtained as follows:

$$g(z) = k_0(C_1 \sinh kz + C_2 \cosh kz + g^*), \tag{69}$$

where g^* is the particular solution related to the shear force $Q(z)$, and C_1 and C_2 are the integration constants related to the boundary conditions.

According to Hooke's law and Equation (61), the stress at any point on the box beam section can be expressed as follows when the influence of the shear deformation of the wing plates and webs is considered.

$$\sigma(x, y, z) = E\left[-y\omega''(z) + \eta(x, y)g'(z)\right] = \frac{yM(z)}{I_x} + \left[\eta(x, y) - \frac{yI_{y\eta}}{I_x}\right]Eg'(z) \tag{70}$$

The equation for the shear lag coefficient λ is as follows:

$$\lambda = \frac{\sigma}{\overline{\sigma}}, \tag{71}$$

where σ represents the actual stress on the section, and $\overline{\sigma}$ represents the stress calculated using the elementary beam theory.

By substituting Equations (6) and (70) into Equation (71), the shear lag coefficients can be expressed as follows:

$$\lambda(x, y, z) = 1 + \left[\frac{\eta(x, y)}{y} - \frac{I_{y\eta}}{I_x}\right] \frac{EI_x g'(z)}{M(z)}. \tag{72}$$

The bending curvature of the girder body is expressed as follows:

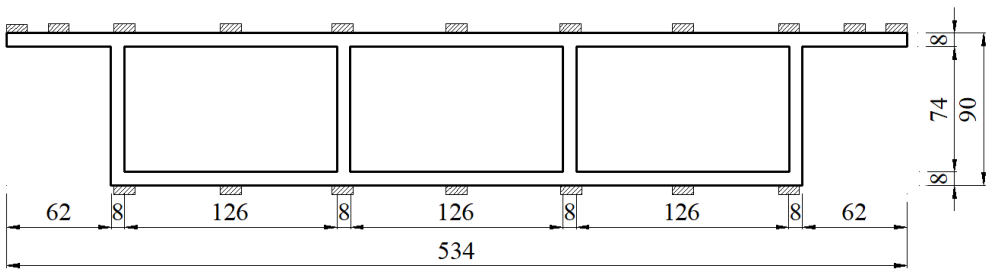
$$\omega'' = -\frac{M(z)}{EI_x} + \frac{I_{y\eta}}{I_x} g'. \tag{73}$$

According to the boundary conditions, the integral constants C_1 and C_2 were solved to determine the expression of the shear displacement, and the theoretical solution of the flexural displacement function of the box girder was obtained by substituting the expression of the shear displacement into Equations (71)–(73).

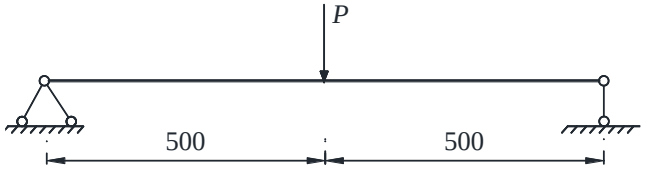
4. Experimental and Case Studies

To validate the displacement function for the flexural strength of the box girders under the influence of the shear deformation in each plate, the results of the theoretical method used in this study were compared with finite-element calculations and experimental measurements for the physical model of an organic-glass, single-box, three-chamber, simply supported box girder [32].

Figure 6 presents the structural dimensions, measurement-point arrangement, and loading effects of the aforementioned Plexiglas simply supported box girder test model [32]. The box girder test model had a span of $L = 1000$ mm. Its elastic modulus and Poisson's ratio, which were measured from a test stretch, were $E = 2600$ MPa and $\nu = 0.385$, respectively. The boundary condition was simulated by supporting steel columns of the same gauge underneath the bottom plates corresponding to all the web ends of the girder. Loads were applied on top of all the webs of the $L/2$ span section of the single-box, three-compartment, simply supported box girder using a loading system. A computer-controlled voltage jack with a load value of $P/4 = 0.4$ kN was used for the centralized force. Photographs of the loading system are shown in Figure 7.



(**a**) Box girder cross-sectional dimensions and measurement-point arrangement.

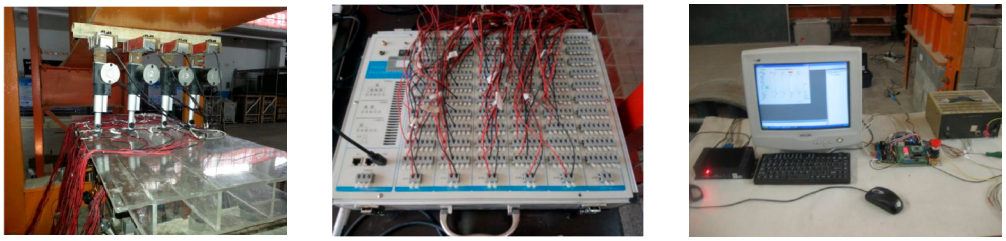


(**b**) Schematic of the model spans and loads.

Figure 6. Schematic of the structural dimensions, measurement points, and loads of the model (unit: mm).

The MIDAS/FEA NX 2021 spatial finite-element software was used to build a solid simulation model of a single-box, three-chamber, simply supported box girder. The cross-section of the finite-element model was a single-box, three-chamber box section. The dimensions and arrangement of the measurement points are shown in Figure 8 and the space finite- element model are shown in Figure 9. Model tests used 120 resistance strain

gauges to measure the longitudinal strain of the box girder under load. A total of 24, 15, and 9 strain gauges were, respectively, arranged on the cross-section, top plate, and bottom plate, and they were affixed to the surface of the box girder using structural adhesive. The measurement points of the finite-element model and locations of the measurement points of the experimental model had a correspondence; the span of the model was $L = 30000$ mm, and the material was C30 concrete with a Young's modulus of $E = 3.0 \times 10^4$ MPa and Poisson's ratio of $\nu = 0.2$. In the finite-element model of the three-chamber box girder, three-dimensional hexahedral solid elements were used to simulate the main girder. The bridge had a total of 234,967 nodes and 157,395 solid units; the centralized load was applied at the top of the 4 webs of the cross-section of the finite-element model of the $L/2$ span, and the value of the load was $P/4 = 360$ kN.



(**a**) Centralized loading (**b**) strain measuring instrument (**c**) Load control system

Figure 7. Loading system used for the model test [32,33].

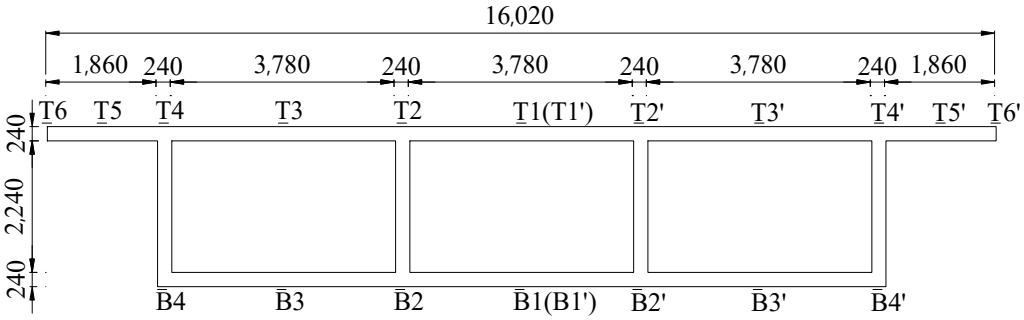


Figure 8. Cross-sectional dimensions and measurement-point arrangement of the finite-element model (unit: mm).

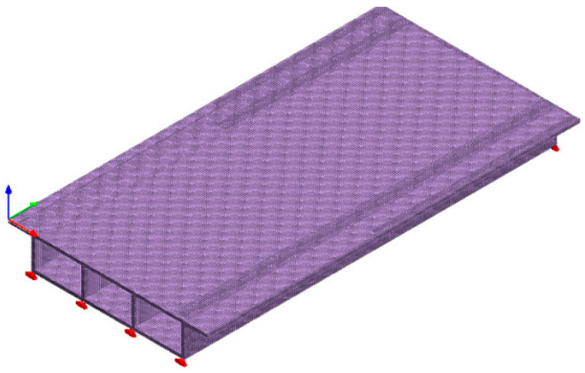


Figure 9. Space finite-element model of plexiglass single-box three-chamber simple support box girder.

According to the similarity principle [34], the cross-sectional stiffnesses corresponding to the finite-element numerical model and the experimental model were similar, as well as their cross-sectional geometries; the load of the finite-element model was proportional to that of the model test, and the model boundary conditions were identical. The results of the theoretical method used in this study are presented in Tables 1 and 2 in comparison with

the finite-element calculation results and the measured values of the model test reported in [32].

Table 1. Comparison of the shear lag coefficients at the key points of the top plate of the $L/2$ and $L/4$ span sections under centralized loading.

Location	Key Point	Theoretical Value	Finite-Element Value	Measured Value
$L/2$ cross-section	T6	0.972	0.846	0.877
	T5	1.001	1.020	0.97
	T4	1.030	1.644	1.098
	T3	0.973	1.066	1.041
	T2	1.037	1.663	1.093
	T1	0.974	1.034	0.842
$L/4$ cross-section	T1′	0.995	1.025	1.323
	T2′	1.007	1.023	1.550
	T3′	0.997	1.004	1.005
	T4′	1.004	0.98	0.988
	T5′	0.999	0.98	0.168
	T6′	0.994	0.977	0.931

Table 2. Comparison of the shear lag coefficients at the key points of the bottom plate of the $L/2$ and $L/4$ span sections under concentrated loading.

Location	Key Point	Theoretical Value	Finite-Element Value	Measured Value
$L/2$ cross-section	B4	1.127	1.153	1.093
	B3	0.905	0.892	0.972
	B2	1.035	1.020	0.993
	B1	0.864	0.871	0.884
$L/4$ cross-section	B1′	0.969	0.965	1.116
	B2′	0.980	0.964	0.97
	B3′	1.003	1.012	0.996
	B4′	1.033	1.041	0.977

As shown in Tables 1 and 2, the theoretically derived flexural displacement function of the thin-walled box girder subjected to bending under the influence of the shear deformation of each plate in this study agreed sufficiently with the measured values of the test and the finite-element numerical simulation values. Most key points of the shear lag coefficient had a relative error of <10.00%. There are several reasons for the occurrence of result discrepancies: firstly, differences in the material properties between the experimental model and the material used in the finite-element numerical simulation; secondly, inherent errors in the experimental setup; thirdly, differences in boundary constraints between the cantilevered plate and the top plate in the model.

5. Correction of Cantilever Plate Displacement for Flexural Displacement Function

Analyzing the finite-element numerical results of the box girder flexural space revealed that when the cantilever of the box girder cantilever plate was longer, the shear lag coefficients of the cantilever plate were significantly smaller than those of the top plate; the difference between the shear lag coefficients at the edge of the cantilever plate and those at the top plate was even larger. To reduce the effect of the stress concentration, the theoretically calculated and finite-element values of the shear lag coefficients in the section at position $y = 1450$ cm of the wing plate were compared; the results are shown in Figure 10.

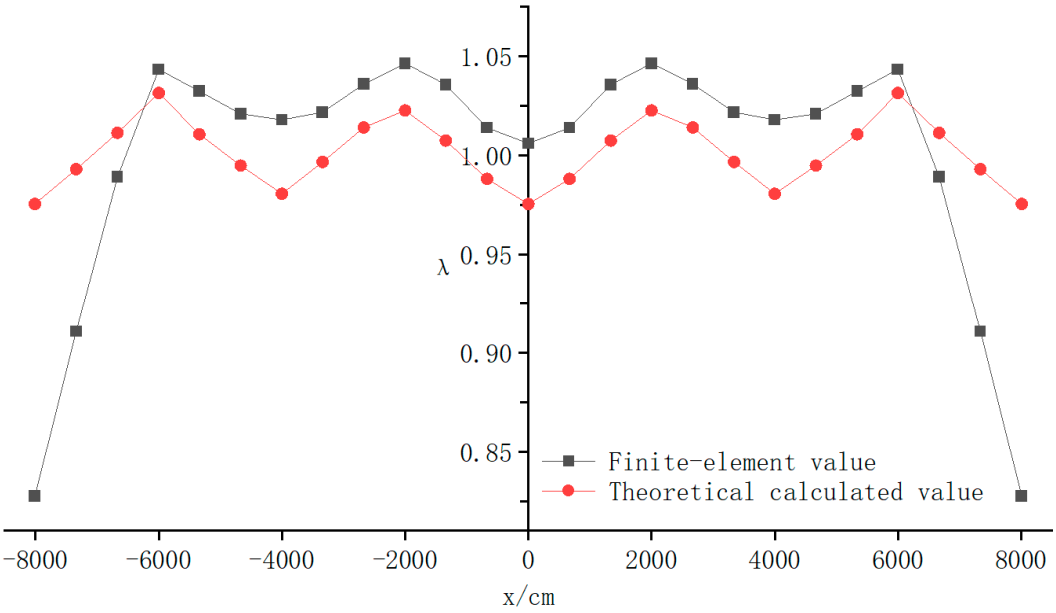


Figure 10. Comparison of the shear lag coefficients of the top wing plate of the section at $y = 1450$ cm for a single-box, three-chamber box girder.

As shown in Figure 10, there was a large difference between the finite-element numerical simulation values at the center of the cantilever plate and the top plate of the box girder and the theoretically calculated values in this study. The shear lag coefficients at the edge of the cantilever plate were smaller than the shear lag coefficients at the center of the top plate, mainly because the edge of the cantilever plate and the center of the top plate had different constraints. Because the cantilever plate at the cantilever end of the constraints did not exist, the top plate of the box chamber on both sides of the web connection was constrained by the different boundary conditions manifested in the difference of the force characteristics. Therefore, it is necessary to optimize the flexural displacement function derived in this study by considering the effect of the shear deformation of each plate and correcting the differences caused by the different boundary constraints. Accordingly, the degree of buckling of the cantilever plate that is corrected using the correction parameter is denoted as φ; Equation (45) is corrected as follows:

$$\eta_\zeta(x,y) = \begin{cases} -y_s\left(b_1{}^2 - x^2\right) - \frac{2q_2}{t}(b_1 - x) + k_1 d & \text{Inner chamber top plate} \\ -y_s\left[4b_2{}^2 - (b_1 + 2b_2 - x)^2\right] - \frac{2q_1}{t}[2b_2 - (b_1 + 2b_2 - x)] + k_1 d & \text{Outer chamber top plate} \\ -y_s\left[b_3{}^2 - (b_1 + 2b_2 + b_3 - x)^2\right]\varphi + k_1 d & \text{Cantilever plate} \\ y_x\left(b_1{}^2 - x^2\right) - \frac{2q_2}{t}(b_1 - x) + k_1 d & \text{Inner chamber bottom plate} \\ y_x\left[4b_2{}^2 - (b_1 + 2b_2 - x)^2\right] - \frac{2q_1}{t}[2b_2 - (b_1 + 2b_2 - x)] + k_1 d & \text{Outer chamber bottom plate} \\ k_1 d & \text{Innerweb} \\ k_2 d & \text{Outer web} \end{cases} \quad (74)$$

The final form of the flexural displacement function of the bent box girder under the influence of the shear deformation of each plate can be obtained by substituting Equation (74) into Equation (39) and applying the axial equilibrium condition. The detailed process is not described herein.

Owing to the influence of the aforementioned parameter φ, the axial equilibrium parameter in Equation (42) can be corrected as follows:

$$d_e = \frac{2\left[(y_s A_t - y_x A_b)\left({b_1}^2 + 4{b_2}^2\right) + (A_t - A_b)\left(\frac{2q_2}{t}b_1 + \frac{2q_1}{t}2b_2\right) + y_s \varphi A_c {b_3}^2\right]}{3A}. \quad (75)$$

In this study, the energy variational method was utilized to analyze the flexural displacement function of the box girder. The expressions of the cross-sectional parameters Equations (49)–(59) in the established control differential equations for the corrected cross-sectional parameters, considering the effect of the correction parameter φ, are as follows:

$$\begin{aligned} A_x = \int_A \left(\frac{\partial \eta_\zeta}{\partial x}\right)^2 dA = \frac{1}{3}\Big\{ & A_t\left[(y_s 2b_1 + 2q_2/t)^2 + (4b_2 y_s + 2q_1/t)^2\right] + \\ & A_b\left[(y_x 2b_1 + 2q_2/t)^2 + (4b_2 y_x + 2q_1/t)^2\right] + A_c(\varphi y_s 2b_3)^2\Big\} \end{aligned} \quad (76)$$

$$\begin{aligned} I_\zeta = {} & \int_A \eta_\zeta(x,y)^2 dA = \left(A_1 {k_1}^2 + A_2 {k_2}^2\right)d^2 + \\ & A_t\left\{\begin{array}{l} \frac{8}{15}\left[{y_s}^2 {b_1}^4 + \left(\frac{q_2 b_1}{t}\right)^2 + {y_s}^2\left(4{b_2}^2\right)^2 + \left(\frac{2q_1 b_2}{t}\right)^2 + \left(\frac{2q_3 b_2}{t}\right)^2\right] - \\ \frac{4}{3}\left(y_s k_1 d {b_1}^2 + y_s k_2 d 4{b_2}^2 - \frac{4y_s q_2 {b_1}^3}{t} - \frac{8y_s q_1 {b_2}^3}{t} - \frac{8y_s q_3 {b_2}^3}{t} + \frac{4k_1 d q_2 b_1}{t} + \frac{2k_2 d q_1 b_2}{t} + \frac{2k_2 d q_3 b_2}{t}\right) \end{array}\right\} + \\ & A_b\left\{\begin{array}{l} \frac{8}{15}\left[{y_x}^2 {b_1}^4 + \left(\frac{q_2 b_1}{t}\right)^2 + {y_x}^2\left(4{b_2}^2\right)^2 + \left(\frac{2q_1 b_2}{t}\right)^2 + \left(\frac{2q_3 b_2}{t}\right)^2\right] + \\ \frac{4}{3}\left(y_x k_1 d {b_1}^2 + y_x k_2 d 4{b_2}^2 - \frac{4y_x q_2 {b_1}^3}{t} - \frac{8y_x q_1 {b_2}^3}{t} - \frac{8y_x q_3 {b_2}^3}{t} + \frac{4k_1 d q_2 b_1}{t} + \frac{2k_2 d q_1 b_2}{t} + \frac{2k_2 d q_3 b_2}{t}\right) \end{array}\right\} + \\ & A_c \varphi y_s\left(\frac{8}{15} y_s {b_3}^2 - \frac{4}{3}k_2 d\right){b_3}^2 \end{aligned} \quad (77)$$

$$I_{n\zeta} = \int_A y^n \eta_\zeta(x,y) dA = \frac{2}{3} {y_s}^{n+1} {y_s}^{n+1}\left[A_t\left({b_1}^2 + 4{b_2}^2\right) + A_c \varphi {b_3}^2 + A_b\left({b_1}^2 + 4{b_1}^2\right)\left(\frac{y_x}{y_s}\right)^{n+1}\right], (n = 1, 3) \quad (78)$$

Here, A_t represents the area of the top plate, A_b represents the area of the bottom plate, A_c represents the area of the cantilever plate, A_w represents the area of one side of the web, and A represents the full cross-sectional area of the box girder.

The equations for the cross-sectional parameters not listed are similar to Equations (53)–(57).

To obtain more accurate values of the shear lag coefficients, the value of the correction parameter φ of the cantilever plate must be determined by comparing the results of the numerical analysis calculations obtained via MIDAS/FEA NX and those obtained via the theoretical method for different values of φ, as well as the calculation of the upper-left wing plate of the finite-element model of a single-box, three-chamber box girder ($x \leq 0$). As shown in Figure 10, the parameter φ must be >1; thus, it was set as 1.0, and increased to 1.7 in steps of 0.1. The shear lag coefficients of the flexural box girder were corrected and calculated, and the results are presented in Table 3.

Table 3. Statistics of the shear lag coefficients of the wing plate at the y = 1450 cm section for the cantilever correction.

x Coordinate (mm)	Finite-Element Value	Correction Parameter φ							
		1.0	1.1	1.2	1.3	1.4	1.5	1.6	1.7
−8010	0.8275	0.9754	0.9614	0.9496	0.9262	0.9049	0.8764	0.8334	0.8014
−7340	0.9107	0.9929	0.9855	0.9801	0.9665	0.9551	0.9398	0.9165	0.8994
−6670	0.9889	1.0112	1.0093	1.0093	1.0039	1.0006	0.9963	0.9898	0.985
−6000	1.0432	1.0313	1.0325	1.036	1.0354	1.0371	1.0394	1.0429	1.0455
−5340	1.0322	1.0105	1.0123	1.0163	1.0167	1.0193	1.0229	1.0282	1.0323

Table 3. *Cont.*

x Coordinate (mm)	Finite-Element Value	Correction Parameter φ							
		1.0	**1.1**	**1.2**	**1.3**	**1.4**	**1.5**	**1.6**	**1.7**
−4670	1.0208	0.9947	0.9968	1.0012	1.0023	1.0055	1.0099	1.0165	1.0215
−4000	1.0178	0.9805	0.9838	0.9895	0.9925	0.9976	1.0046	1.0150	1.0227
−3340	1.0216	0.9965	0.9987	1.0034	1.0047	1.0084	1.0132	1.0205	1.0260
−2670	1.0358	1.0139	1.0159	1.0203	1.02123	1.0244	1.0287	1.0352	1.0400
−2000	1.0462	1.0225	1.0247	1.0294	1.0307	1.0345	1.0394	1.0470	1.0524
−1340	1.0355	1.0073	1.0098	1.0145	1.0161	1.0201	1.0253	1.0331	1.0389
−670	1.0138	0.988	0.9907	0.9956	0.9975	1.0016	1.0071	1.0154	1.0216
0	1.0059	0.9753	0.9785	0.9837	0.9862	0.9907	0.9970	1.0063	1.0132

As shown in Table 3, when the value of the cantilever modification parameter φ is 1.6, according to the flexural displacement function derived in this study, the calculated shear lag coefficient values of the wing plate on the box girder at each point optimally coincide with the numerical simulation results of MIDAS/FEA NX and fully reflect the distribution law, indicating that the shear lag coefficient of the cantilever plate is smaller than that of the top plate. To more intuitively examine the influence of the correction parameter φ, the shear lag coefficient values of the wing plate on the box girder at the $y = 1450$ cm section were compared, as shown in Figure 11.

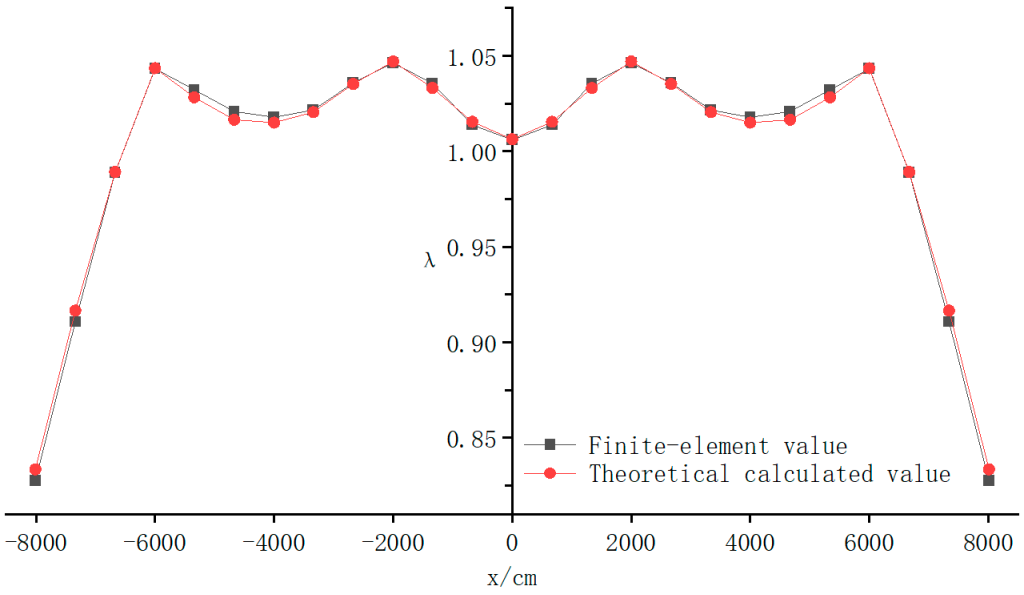


Figure 11. Comparison of the flexural stresses in the upper-wing plate of the box girder at $y = 1450$ cm for a single-box three-chamber box girder at $\varphi = 1.6$.

Comparing the stress distributions shown in Figures 10 and 11 reveals that when the cantilever plate correction parameter φ had a value of 1.6, the stresses on the upper-wing plate of the box girder calculated via the proposed theoretical method and the results obtained via the MIDAS/FEA NX numerical simulation agreed well, and the relative difference in the data was <2.00%. The proposed theoretical method can fully reflect the different constraint conditions of the cantilever plate and the top plate, as well as the transverse distribution of the stresses along the wing plate.

6. Discussions

Based on the experimental model of an acrylic single-box three-chamber box beam and a solid finite-element model established using MIDAS/FEA NX, stress and deflection at key points of sections $L/2$ and $L/4$ of the simply supported box beam under different loading

conditions were analyzed. The results of the normal stress and beam deflection obtained by solving the deflection function using the energy variational method were compared and analyzed against the finite-element numerical simulation results and experimental measurements. By comparing the stress results, significant discrepancies were found at the edge of the cantilevered plate when using the energy variational method to solve the deflection function. After correcting for the displacement of the cantilevered plate in consideration of the shear deformation effects on each plate, the results were compared with finite-element analysis. The conclusion is as follows:

(1) Comparing the experimental measurements, finite-element simulation values, and theoretical method calculations, the data results show good agreement, with the vast majority of data discrepancies within 10.00%. This confirms the reliability of the deflection function derived in this paper for the bending box beam considering the shear deformation effects on each plate.

(2) Due to different boundary constraints at the edge of the cantilevered plate and at the center of the top plate, the cantilevered plate and the top plate exhibit differences in two-dimensional stress characteristics and boundary constraints. By calculating the boundary conditions of the cantilevered plate for the deflection function of the bending box beam considering the shear deformation effects on each plate, when the cantilevered plate correction parameter is $\varphi = 1.6$, the theoretical method aligns most closely with the finite-element simulation results, with a relative discrepancy of less than 2.00%.

7. Conclusions

For the thin-walled box girder under the action of the shear deformation of each plate, the flexural displacement function of the wing and web plates of the box girder cannot satisfy the assumption of the plane section; the longitudinal flexural displacement function in the transverse direction of the wing plate is a quadratic function, and the height of the web plate is the sum of the primary and cubic functions.

According to the theoretical analysis of the axial equilibrium conditions of the thin-walled box girder subjected to bending under the influence of the shear deformation of each plate, the actual neutral axis of the box girder under the influence of shear deformation no longer coincides with the horizontal axis of the box girder cross-section, having an offset distance of $d \times g(z)$.

The measured values of the model test, the simulated values of the finite-element model, and the calculated values of the theoretical method were compared, revealing sufficient agreement among the results. The majority of the shear lag coefficients had a relative error of <10.00%, confirming that the flexural displacement function of the flexural box girder under the influence of the shear deformation of the various plates derived in this study is reliable.

Owing to the different constraint conditions at the edge of the cantilever plate and at the center of the top plate, the cantilever plate and top plate exhibit differences in their two-dimensional force characteristics and boundary constraints. The length of the cantilever plate should be appropriately reduced in engineering design to weaken its influence on the shear lag effect of the box girder.

The article investigates the theoretical solution of shear hysteresis effects in bent box girders based on the energy method, along with the influencing factors of shear hysteresis effects. An empirical formula for shear hysteresis effects in single-box three-chamber box girders is fitted using Origin, addressing the issue of workload in calculating internal forces of box girders. In future developments, the following issues will continue to be addressed:

During the derivation of the deflection function for thin-walled box girders, local constraints such as bulkheads and fillet welds were not considered. In future work, it is necessary to conduct a thorough analysis of the effects of these local constraints.

As box girder structures continue to evolve towards wider cantilevered plates, larger flange-rib spacings, and lighter thin-walled materials, the nonlinear effects in geometric structure and material properties will become increasingly significant. This will become

a major research area for thin-walled box girders in the future, requiring further study to refine the theoretical calculations for thin-walled box girders.

Author Contributions: Conceptualization, methodology, software, and validation, formal analysis, investigation, resources, data curation, Y.L. (Yanfeng Li) and J.X.; writing—original draft preparation, writing—review and editing, visualization, Y.L. (Yanfeng Li) and F.W.; supervision, project administration, funding acquisition, F.W. and Y.L. (Yuanhui Li). All authors have read and agreed to the published version of the manuscript.

Funding: This work was supported by National Key R&D Program of China (Nos. 2018YFC0809600 and 2018YFC0809606); Natural Science Foundation of Liaoning Province (No. 2019-MS-265); and Key Laboratory of the Ministry of Education on Safe Mining of Deep Metal Mines (No. 2019SMDM-KF-A01); Shenyang Municipal Science and Technology Planning Project Fund (No. 23-407-3-19).

Institutional Review Board Statement: Not applicable.

Informed Consent Statement: Not applicable.

Data Availability Statement: Data used to support the findings of this study are available from the corresponding author upon request.

Conflicts of Interest: The authors declare no conflicts of interest.

References

1. Zhou, S. Effect of Shear Lag on Structural Behaviours in Indeterminate Box-Girders. *J. Civ. Archit. Environ. Eng.* **2010**, *32*, 7–11. [CrossRef]
2. Luo, Z.; Song, Y.; He, S.; Huang, F. Combined Element Method for Shear Lag Effect Analysis of Thin-walled Box Girder. *J. Highw. Transp. Res. Dev.* **2014**, *31*, 58–63+75. [CrossRef]
3. Zhang, Y.; Liu, Z.; Wang, C. Rational Method for Computing Polar Inertia Moment of Thin-walled Box Girders with Cantilever Slab. *J. China Railw. Soc.* **2019**, *41*, 94–99. [CrossRef]
4. Chen, Y.; Dong, J.; Xu, T.; Xiao, Y.; Jiang, R.; Nie, X. The shear-lag effect of composite box girder bridges with corrugated steel webs and trusses. *Eng. Struct.* **2019**, *181*, 617–628. [CrossRef]
5. Zhou, S. Finite beam element considering shear-lag effect in box girder. *J. Eng. Mech.* **2010**, *136*, 1115–1122. [CrossRef]
6. Luo, Q.; Wu, Y.; Li, Q.; Tang, J.; Liu, G. A finite segment model for shear lag analysis. *Eng. Struct.* **2004**, *26*, 2113–2124. [CrossRef]
7. Wei, C.; Li, B.; Zeng, Q. Transfer Matrix Method Considering Both Shear Lag and Shear Deformation Effects in Non-Uniform Continuous Box Girder. *Eng. Mech.* **2008**, *25*, 111–117.
8. Ding, N.; Lin, L.; Qian, Y. An Approximate Method to Analyze the Effect of Shear Lag and Shear Deformation of Box Beam with Varying Depth. *J. Railw. Sci. Eng.* **2011**, *8*, 14–18.
9. Chen, D.; Xu, Z.; Wang, Y. Derivation of Stiffness Matrix of Variable Section Beam Element Based on Energy Variation Method. In Proceedings of the 2019 Exchange Meeting on New Materials, Technologies and Their Engineering Applications in Civil Engineering, Beijing, China, 17 May 2019; Zhengzhou University: Zhengzhou, China, 2019; pp. 1639–1645.
10. Zhang, Y.; Zhang, Y.; Zhang, H. Influence of Lateral Displacement of Flanges on Shear Lag Effect of Box Girder. *J. Southeast Univ. (Nat. Sci. Ed.)* **2022**, *52*, 247–253. [CrossRef]
11. Lin, P.; Zhou, S.; Liu, F. Additional Axial Force Analysis Caused by Parabolical Warping Displacement about Shear Lag. *Eng. Mech.* **2010**, *27*, 90–93+109. Available online: https://pubs.cstam.org.cn/article/id/em_1213 (accessed on 1 August 2010).
12. Song, A.; Li, Z.; Zhou, P.; Wang, S.; Su, Q. Analysis of Shear Lag Effect in Thin-walled Box Girder Based on Cosine Warping Displacement Function. *Highw. Eng.* **2021**, *46*, 12–18. [CrossRef]
13. Guo, W.; Yang, Z.; Feng, Q.; Dai, C.; Yang, J.; Lei, X. A new method for band gap analysis of periodic structures using virtual spring model and energy functional variational principle. *Mech. Syst.* **2022**, *168*, 683–692. [CrossRef]
14. An, H.; Wu, X.; Shi, Y.; Yin, Y. Theoretical analysis of shear lag warping displacement function of box girder. *Eng. J. Wuhan Univ.* **2020**, *53*, 692–697. [CrossRef]
15. Lin, P.; Liu, F.; Yang, J.; Ji, W.; Liu, Y. Definition and Application of Shear-lag Warping Displacement Functions for Box Girders. *Chin. J. Comput. Mech.* **2012**, *29*, 789–794. Available online: https://pubs.cstam.org.cn/article/id/cjcm_jslxxb201205025 (accessed on 1 October 2010).
16. Penalba, M.; Ulazia, A.; Ibarra-Berastegui, G.; Ringwood, J.; Sáenz, J. Wave energy resource variation off the west coast of Ireland and its impact on realistic wave energy converters' power absorption. *Appl. Energy* **2018**, *224*, 205–219. [CrossRef]
17. Lu, P.; Li, D.; Zhang, Y.; Zhou, Y. Bending characteristics of composite box girder considering all surfaces shear deformation based on Hamiltonian system. *Mech. Based Des. Struct. Mach.* **2023**, *51*, 2583–2606. [CrossRef]
18. Zhang, Y.; Hu, Y.; Lin, L. Analysis on Shear Lag Effect of Thin-Walled Box Girders Based on A Modified Warping Displacement Mode. *China Civ. Eng. J.* **2015**, *48*, 44–50.

19. Elshazli, M.T.; Abdulazeez, M.M.; ElGawady, M.; Ibrahim, A. Comprehensive Numerical Modeling of Prestressed Girder Bridges under Low-Velocity Impact. *Buildings* **2024**, *14*, 640. [CrossRef]
20. Maleska, T.; Beben, D. Behaviour of soil–steel composite bridges under strong seismic excitation with various boundary conditions. *Materials* **2023**, *16*, 650. [CrossRef]
21. Jing, Y.; Zhang, X.; Zhou, Y.; Zhao, Y.; Li, W. Dynamic response and impact force calculation of PC box girder bridge subjected to over-height vehicle collision. *Buildings* **2023**, *13*, 495. [CrossRef]
22. Wang, Q.; Dai, R.; Wang, S.; Wang, Y. Prediction Algorithm and Interpretation for Autogenous Shrinkage of Concrete Based on Machine Learning. *J. Shenyang Jianzhu Univ.* **2023**, *39*, 1050–1057.
23. Zhou, M.; Zhang, Y.; Lin, P.; Zhang, Z. A new practical method for the flexural analysis of thin-walled symmetric cross-section box girders considering shear effect. *Thin-Walled Struct.* **2022**, *171*, 108710. [CrossRef]
24. Huang, J. *Torsional Analysis of Thin-Walled Structures: Curved Beams and Diagonally Supported Box Girders*; China Railway Publishing House: Beijing, China, 1988.
25. Gupta, T.; Kumar, M. Flexural response of skew-curved concrete box-girder bridges. *Eng. Struct.* **2018**, *163*, 358–372. [CrossRef]
26. Shan, Z. *Mechanics of Materials*, 3rd ed.; Higher Education Press: Beijing, China, 2016.
27. Cai, J.; Moen, C. Elastic buckling analysis of thin-walled structural members with rectangular holes using generalized beam theory. *Thin-Walled Struct.* **2016**, *107*, 274–286. [CrossRef]
28. Guo, J. *Theory of Box Girder Design*, 2nd ed.; People's Transportation Publishing House: Beijing, China, 2008.
29. Bao, S. *Structural Mechanics of Thin-Walled Bars*; China Architecture Publishing & Media: Beijing, China, 2016.
30. Dym, C.; Shames, I. *Utilixue Blanfenfa*; China Railway Publishing House: Beijing, China, 1984.
31. Lai, Z.; Jiang, L.; Zhou, W.; Liu, X.; Yu, J.; Zhang, Y. Analytical soluteon to mapping rail deformation under bridge transverse deformation using energy variational principle. *J. Cent. South Univ.* **2022**, *29*, 2654–2664. [CrossRef]
32. Luo, M.; Lin, P. Experimental Study of Shearing Force Lag Effect of Three-cell Box Girder. *J. Exp. Mech.* **2015**, *30*, 621–628. [CrossRef]
33. Zhang, K. The Theoretical and Experimental Investigations on the Space Mechanical Behavior of Single Box and Triple Cells Girder under Symmetrical Load. Master's Thesis, Lanzhou Jiaotong University, Lanzhou, China, 2017; 67p. Available online: https://cdmd.cnki.com.cn/Article/CDMD-10732-1018234535.htm (accessed on 3 June 2017).
34. Chu, F.; Cao, P.; Wan, L. Similarity Theory and Its Application to Simulation Tests. *Min. Technol.* **2007**, *4*, 64–65+78. [CrossRef]

Disclaimer/Publisher's Note: The statements, opinions and data contained in all publications are solely those of the individual author(s) and contributor(s) and not of MDPI and/or the editor(s). MDPI and/or the editor(s) disclaim responsibility for any injury to people or property resulting from any ideas, methods, instructions or products referred to in the content.